Journal of Alzheimer's Disease 47 (2015) 509–522
DOI 10.3233/JAD-150184
IOS Press

Identification of Amnestic Mild Cognitive Impairment Using Multi-Modal Brain Features: A Combined Structural MRI and Diffusion Tensor Imaging Study

Yunyan Xie[a,1], Zaixu Cui[b,1], Zhongmin Zhang[c,1], Yu Sun[a], Can Sheng[a], Kuncheng Li[d], Gaolang Gong[b,*], Ying Han[a,e,*] and Jianping Jia[a,e,f,*]
[a]*Department of Neurology, Xuan Wu Hospital of the Capital Medical University, Beijing, China*
[b]*State Key Laboratory of Cognitive Neuroscience and Learning & IDG/Mc Govern Institute for Brain Research, Beijing Normal University, Beijing, China*
[c]*Department of Neurology, Hongqi Hospital, Mudanjiang Medical College, Mudanjiang, Heilongjiang, China*
[d]*Department of Radiology, Xuan Wu Hospital of the Capital Medical University, Beijing, China*
[e]*Center of Alzheimer's Disease, Beijing Institute for Brain Disorders, China*
[f]*Beijing Key Laboratory of Geriatric Cognitive Disorders and Neurodegenerative Laboratory of Ministry of Education of the People's Republic of China, Beijing, China*

Accepted 27 April 2015

Abstract. Identifying amnestic mild cognitive impairment (aMCI) is of great clinical importance because aMCI is a putative prodromal stage of Alzheimer's disease. The present study aimed to explore the feasibility of accurately identifying aMCI with a magnetic resonance imaging (MRI) biomarker. We integrated measures of both gray matter (GM) abnormalities derived from structural MRI and white matter (WM) alterations acquired from diffusion tensor imaging at the voxel level across the entire brain. In particular, multi-modal brain features, including GM volume, WM fractional anisotropy, and mean diffusivity, were extracted from a relatively large sample of 64 Han Chinese aMCI patients and 64 matched controls. Then, support vector machine classifiers for GM volume, FA, and MD were fused to distinguish the aMCI patients from the controls. The fused classifier was evaluated with the leave-one-out and the 10-fold cross-validations, and the classifier had an accuracy of 83.59% and an area under the curve of 0.862. The most discriminative regions of GM were mainly located in the medial temporal lobe, temporal lobe, precuneus, cingulate gyrus, parietal lobe, and frontal lobe, whereas the most discriminative regions of WM were mainly located in the corpus callosum, cingulum, corona radiata, frontal lobe, and parietal lobe. Our findings suggest that aMCI is characterized by a distributed pattern of GM abnormalities and WM alterations that represent discriminative power and reflect relevant pathological changes in the brain, and these changes further highlight the advantage of multi-modal feature integration for identifying aMCI.

Keywords: Alzheimer's disease, amnestic mild cognitive impairment, classification, diffusion tensor imaging, structural magnetic resonance imaging, support vector machine

[1]These authors contributed equally to this work.

*Correspondence to: Jianping Jia, Department of Neurology, Xuan Wu Hospital of the Capital Medical University, Beijing 100053, China. Tel.: +86 10 83198730; Fax: +86 10 83171070; E-mail: jiajp@vip.126.com.; Ying Han, Department of Neurology, Xuan Wu Hospital of the Capital Medical University, Beijing 100053, China. Tel.: 13621011941; E-mail: 13621011941@163.com.; Gaolang Gong, PhD, State Key Laboratory of Cognitive Neuroscience and Learning & IDG/McGovern Institute for Brain Research, Beijing Normal University, Beijing 100875, China. Tel.: +86 1058804678; Fax: +86 1058806154; E-mail: gaolang.gong@bnu.edu.cn.

ISSN 1387-2877/15/$35.00

Table 1
Demographics and behavioral profiles of the aMCI and the NC groups

	aMCI Group ($n = 64$)	NC Group ($n = 64$)	Group Comparison (p values)
Gender (M/F)	28/36	26/38	0.723[a]
Age, years	67.141 ± 9.304	64.797 ± 7.595	0.121[b]
Education, years	9.891 ± 4.254	11.078 ± 4.887	0.145[b]
MMSE	23.781 ± 3.089	28.016 ± 2.229	<0.0001[b]
MoCA	19.122 ± 3.592	25.979 ± 3.173	<0.0001[b]
CDR	0.5	0	–
AVLT-Immediate Recall 1	3.625 ± 1.507	7.000 ± 2.218	<0.0001[b]
AVLT-Immediate Recall 2	5.172 ± 1.760	9.531 ± 2.330	<0.0001[b]
AVLT-Immediate Recall 3	6.156 ± 1.913	10.766 ± 2.238	<0.0001[b]
AVLT-Delayed Recall	3.000 ± 2.404	9.969 ± 3.013	<0.0001[b]
AVLT-Recognition	6.953 ± 3.731	11.703 ± 3.120	<0.0001[b]

aMCI, amnestic Mild Cognitive Impairment; NC, Normal Control; MMSE, Mini-Mental State Examination; MoCA, Montreal Cognitive assessment; CDR, Clinical Dementia Rating Scale; AVLT, Auditory Verbal Learning Test. Age, education, MMSE, MoCA, and AVLT are presented as the mean ± SD. [a]The p value was obtained using a two-tail chi-square test. [b]The p value was obtained using a two-sample two-tail t test. Fifteen aMCI patients and 17 controls did not have MoCA scores.

INTRODUCTION

Alzheimer's disease (AD) is a degenerative disease that accounts for the majority of patients with dementia. With the population aging, the incidence of AD has substantially increased [1, 2]. As a putative prodromal stage of AD, amnestic mild cognitive impairment (aMCI) has attracted much attention. Early interventions for aMCI have been demonstrated to be capable of decreasing or delaying the development of AD [3]. Therefore, accurately identifying aMCI patients is of great clinical value. To facilitate the identification of aMCI, objective neurobiological markers, e.g., those derived from neuroimaging techniques, are highly desirable.

Machine learning and pattern recognition techniques have been used to explore the potential neuroimaging biomarkers of aMCI. With these techniques, several imaging modalities have been used to discriminate aMCI patients from normal controls. For example, some studies have employed structural magnetic resonance imaging (sMRI) data to extract cortical morphological information (e.g., cortical volumes and cortical thickness) to distinguish aMCI patients from controls [4, 5], and the characterizations of white matter (WM) microstructures and whole-brain anatomical connectivity based on diffusion tensor imaging (DTI) data have been used to identify aMCI patients [6, 7].

However, the majority of discriminative studies of aMCI have focused on a single modality. Multiple modalities might provide complementary information. For example, sMRI data contain rich morphological information about the brain tissues and have been widely used to study GM abnormalities in aMCI patients [8, 9], whereas DTI data can be used to index the different microstructural properties of the WM, and many studies have reported that there was reduced fractional anisotropy (FA) and increased mean diffusivity (MD) in aMCI patients compared to normal controls [7, 10].

The current study explored the feasibility of integrating structural MRI and DTI to more accurately distinguish aMCI patients from controls. To date, only one published study, to our knowledge, has used both sMRI and DTI for aMCI classification. However, this study reported limited predictive power (accuracy: 71.09% and sensitivity: 51.96%) [11]. The low accuracy of this study might have been related to the feature definitions, which were based on the neuroimaging metrics of a limited number of regions of interest. To overcome this limitation, the present study integrated whole-brain voxel-based maps, which were acquired from both sMRI and DTI, as features to identify aMCI patients. Specifically, a fused classifier was applied to a large cohort of Han Chinese with aMCI and control subjects.

MATERIALS AND METHODS

Participants

Seventy-three aMCI patients and 72 matched normal controls (NC) participated in this study. All subjects were right-handed native Chinese speakers. The aMCI subjects were all recruited from the memory clinic at Xuan Wu Hospital, Beijing, China, and the NC subjects were recruited from nearby communities. Written informed consent was obtained from all sub-

jects before data collection. This study was approved by the Research Ethics Review Board of Xuan Wu Hospital. The current study is a sub-project of a larger research project, and the detailed inclusion and exclusion criteria for the aMCI patients and controls have been described in our previous papers [4, 12]. Confirmation of diagnosis for all subjects was made by the consensus of at least two experienced neurologists in the Neurology Department of Xuan Wu Hospital. The diagnoses were based on the available data from the neuropsychological assessment evaluation, a battery of general neurological examinations, collateral and subject symptoms as well as functional capacity reports. Specifically, all aMCI subjects met the following inclusion criteria: (1) memory complaints, preferably confirmed by an informant; (2) objective memory impairment adjusted for age and education; (3) normal or near-normal performance in general cognitive functioning and no, or minimal, impairments of daily life activities; (4) a Clinical Dementia Rating (CDR) score of 0.5; and (5) not meeting the criteria for dementia from the Diagnostic and Statistical Manual of Mental Disorders, fourth edition, revised (DSM-IV). The controls did not have psychiatric or neurological illnesses, which was confirmed using the Structured Interview for DSM-IV Non-Patient Edition. Subjects with any of the following clinical characteristics, which were assessed based on clinical evaluations and medical records, were excluded: (1) vascular cognitive impairment (Hachinski ischemic scale score $\geq$4 points); (2) severe depression (Hamilton Depression Rating Scale score >24 points); (3) other neurological disorders, including a brain tumor, traumatic brain injury, Parkinson's disease, encephalitis or epilepsy; (4) other systemic diseases, such as thyroid dysfunction, severe anemia, chronic diarrhea and malnutrition, liver or kidney dysfunction, carbon monoxide poisoning, syphilis or human immunodeficiency virus infection; (5) a history of psychosis or congenital mental growth retardation; (6) obvious abnormalities in magnetic resonance images, such as leukoaraiosis and infarction; (7) alcohol or drug abuse; (8) obvious impairments of daily life activities (Activity of Daily Living Scale score $\geq$23 points if age <75, or $\geq$25 points if age $\geq$75); and (9) severe hearing or vision impairment that made the subject unable to cooperate with examinations.

Two aMCI patients and two controls lacked DTI data whereas one aMCI patient lacked sMRI data. These individuals were removed from the study. Additionally, two aMCI patients and four controls were excluded because the scanning parameters of their sMRIs were inconsistent with others. However, there was a significant difference in age of the remaining subjects between the two groups. We used the intersection of the age range for the two groups (47 75) as the threshold and removed individuals whose age was out of this range. Therefore, four aMCI subjects and two controls were excluded. Overall, 64 aMCI participants and 64 NC were included in the analysis. The clinical and demographic data for these participants are shown in Table 1.

Image acquisition

All scans were performed using the 3-T Siemens Tim Trio MRI scanner in Xuan Wu Hospital, Beijing, China. Three-dimensional, high-resolution, T1-weighted images were obtained using a three-dimensional magnetization prepared rapid gradient echo (MP-RAGE) sequence with the following parameters: slice thickness, 1 mm; no gap; 176 sagittal slices; repetition time (TR), 1900 ms; echo time (TE), 2.2 ms; flip angle, 9°; acquisition matrix, 256×224; field of view (FOV), 256×224 mm^2; and resolution, $1 \times 1 \times 1$ mm^3. The DTI data were acquired using a single-shot echo-planar imaging-based sequence with the following parameters: slice thickness, 2 mm; no gap; 60 axial slices; TR, 11000 ms; TE, 98 ms; flip angle, 90°; one acquisition for 17 subjects and three repetitive acquisitions for the other 111 subjects; acquisition matrix, 128×116; FOV, 256×232 mm^2; resolution, $2 \times 2 \times 2$ mm^3; and 30 non-linear diffusion weighting directions with b = 1000 s/mm^2 and one image without diffusion weighting (i.e., b = 0 s/mm^2). According to the MRI images, there were small infarctions or white matter hyperintensity in individuals from both the aMCI and the NC groups, but there was not a noticeable group difference in the frequency or spatial locations of these phenomena within the brain.

Image preprocessing (Feature extraction)

Gray matter volume (GMV)

For each individual, a GMV map in the MNI space was generated using the VBM8 toolbox (http://dbm.neuro.uni-jena.de/vbm/) in SPM8 (http://www.fil.ion.ucl.ac.uk/spm/). Specifically, the following processing steps were completed: (1) each subject's image was normalized to a template and then segmented into GM, WM, and cerebrospinal fluid using the New Segment toolbox [13]; (2) The GM partition was registered to a custom template using DARTEL (Diffeomorphic Anatomical Registrations Through Exponentiated Lie

Algebra) with a default template with a $1.5 \times 1.5 \times 1.5$ mm^3 resolution [14]; and (3) affine transformation and non-linear warping were applied to modulate normalized GM and the GMV maps were acquired in the standard space. In the GMV map, the value of each voxel represents the absolute volume of GM in the native space. Next, the acquired GMV map with a voxel size of $1.5 \times 1.5 \times 1.5$ mm^3 was smoothed with a 6-mm Gaussian kernel.

WM diffusion metrics

The processing of the DTI dataset was implemented with PANDA (http://www.nitrc.org/projects/panda), which is a Matlab toolbox for the pipeline analysis of diffusion images [15]. Briefly, the data processing included the following: (1) skull removal and brain mask estimation; (2) eddy-current and head motion correction; (3) averaging of three acquisitions for the 111 subjects and using one acquisition for the other 17 subjects; (4) calculation of the diffusion tensor metrics; and (5) registration of all of the individual images to a standard space with a target voxel size of $2 \times 2 \times 2$ mm^3. Finally, the FA and MD images were smoothed with a 6-mm Gaussian kernel.

After data preprocessing, the GMV, FA, and MD maps that represent GM volume, fiber organization/directionality and tissue density, respectively, were acquired. To remove unneeded voxels, averaged GMD and FA maps were produced across all subjects, and a threshold value of 0.2 was applied to both the averaged GMD and FA maps. A GM mask and a WM mask were obtained. The following GMV analysis was restricted to the GM mask, and the FA/MD analysis was restricted to the WM mask.

Discriminative analysis

The flowchart of the proposed classification framework is shown in Fig. 1. Specifically, feature selection was applied to select a small set of features for each metric (i.e., GMV, FA, and MD). Next, three support vector machine (SVM) classifiers were trained with the selected features, and the sum rule was applied to combine their decisions. Leave-one-out and 10-fold cross-validations were used to estimate the performance of the classifiers. Finally, we identified the most discriminative features.

Feature selection

Each voxel in the GMV, FA, or MD map was a feature for classifying the aMCI and the control groups in the present study. The dimensionality of the feature space was high and non-informative noise was

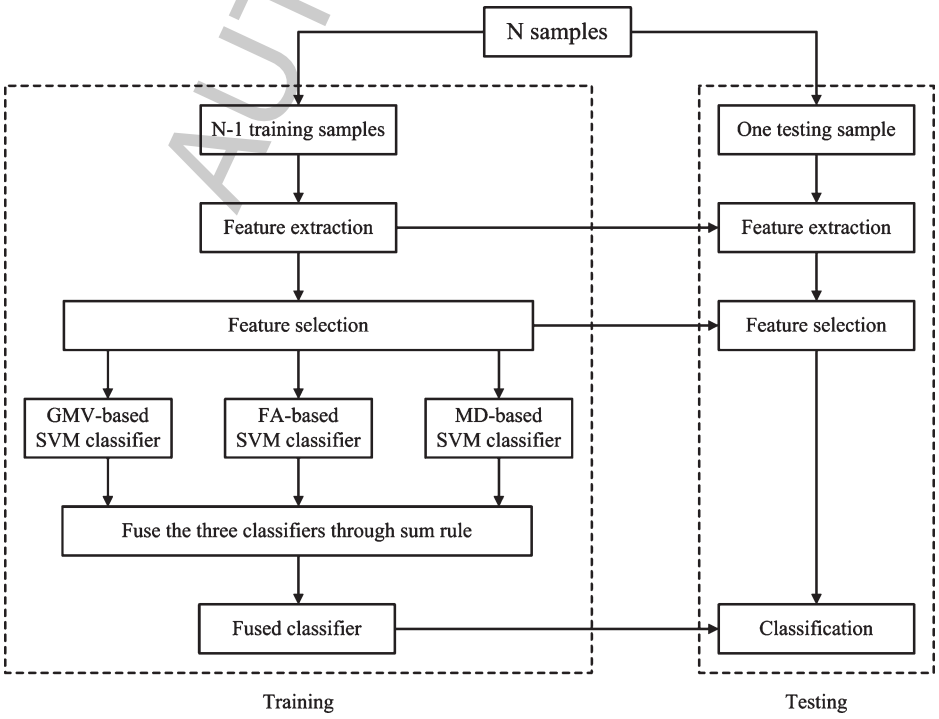

Fig. 1. The flowchart of the proposed classification framework.

present. Many studies have demonstrated that removing these non-informative features always improves classification performance [16, 17]. Therefore, univariate filtering was adopted in this study for feature selection. Specifically, a two-sample, two-tailed *t*-test was applied to each voxel, and the features with significant differences ($p < 0.05$, uncorrected) were retained [18, 19]. This feature selection process was performed on the training set to avoid over-fitting the classifier.

SVM-based classification

Linear SVM was used to classify the aMCI and NC groups based on the three metrics (GMV, FA, and MD). SVMs [20] are currently the most widely used supervised learning method. They minimize empirical classification errors by taking into account the complexity of the model. The complexity was controlled by identifying the hyperplane with the maximum margin. The margin is the distance separating the hyperplane from the closet training samples, which are called support vectors. These support vectors specify the final separating hyperplane. The linear SVM was used in this study to avoid over-fitting and to allow for the direct extraction of the weight vectors as indices of the importance of the features. The parameter C, which controls the trade-off between empirical classification errors and the complexity of the model, was set at the default value (C = 1). The LIBSVM toolbox for Matlab was used to perform the linear SVM classification (http://www.csie.ntu.edu.tw/ cjlin/libsvm/) [21].

Classifier fusion

Generally, a fused classifier that combines the predicted results of multiple classifiers can achieve superior performance if the base classifiers are accurate and diverse [22–24]. Model diversity, which is the key feature of fused classifiers, indicates the extent to which the individual classifiers make errors in different instances. A commonly used method of adding diversity is to combine several different metrics that reflect different aspects and might complement each other [18, 25]. A fused classifier that combined the three classifiers (i.e., the GMV-based, FA-based and MD-based classifiers) via the sum rule was used in this study [22]. The final label was determined by the sum of the classification score for each base classifier ($y = wx+b$):

$$F(x_i) = sign\left(\sum_{k=1}^{3} y_k(x_i^k)\right) \quad (1)$$

where $x_i = \left\{x_i^k,\ k = 1,\ 2,\ 3\right\}$ is a feature vector of the three metrics of the i-th test sample, x_i^k is a feature vector of the k-th metric, y_k is the classification score of its corresponding classifier, and $F(x_i)$ is the final label of the *i*-th test sample.

Performance evaluation

Leave-one-out cross-validation (LOOCV) was used to validate the performance of the classifiers. LOOCV can provide a good estimation of the generalizability of the classifiers [4, 17]. In each LOOCV fold, one subject was first left out as the testing subject, and the remaining subjects were used for training a fused classifier. Next, the classifier was used to classify the testing subject. This procedure was repeated such that each subject in the sample was used once as the testing subject.

Additionally, we also evaluated the fused classifier using 10-fold cross-validation. Specially, the full data set was randomly partitioned into 10 subsets, of which 1 subset was used as the test data, and the remaining 9 subsets were used as training data. This procedure was repeated 10 times to make sure each fold has been used once as the testing set. Because the full data were randomly divided into 10 subsets, the performance may depend on the data division. Therefore, the 10-fold cross-validation was repeated 100 times, and the results were averaged to produce a final classification performance.

Accuracy, sensitivity, specificity, positive predictive value (PPV), and negative predictive value (NPV) were used as quantitative assessments of the generalizability of the classifier. Accuracy is the proportion of subjects that were correctly classified into the aMCI or the NC group. Sensitivity and specificity were the proportions of the aMCI and the NC participants who were correctly classified, respectively. PPV and NPV were the proportions of correct aMCI predictions and NC predictions, respectively.

A receiver operating characteristics (ROC) graph was also employed to evaluate the performance of the classifier [26]. Taking each subject's classification score as a threshold, the ROC graph of the fused classifier was visualized. The area under a ROC curve (AUC) is a commonly used quantitative assessment of the diagnostic power of a predictive model.

The permutation test was applied to determine whether the accuracy and the AUC of the fused classifier were significantly higher than the values expected by chance. Specifically, we permuted the class labels (aMCI or control) across the entire sample 2,000 times without replacement, and each time we performed the entire LOOCV classification process. The *p* value for the accuracy or AUC was calculated by dividing the

number of permutations that showed a higher value than the actual value for the real sample by the total number of permutations (i.e., 2,000).

The most discriminative features

In each fold of the LOOCV, the feature selection was based on a slightly different subset of the data. Therefore, the selected features differed slightly from fold to fold. The relevant features were restricted to those that appeared in every fold of the LOOCV for each base classifier [18, 19]. Additionally, it is well established that the weight vector of a linear SVM classifier, which has the same dimensions as the feature vector and is normal to the hyperplane, represents the discriminative power of the features [27, 28]. The weight of these relevant features is the average of the absolute weight across all folds. The most discriminative features were restricted to the first 20% relevant features with the greatest weights. This threshold can eliminate noise components to some extent, thus enabling better concentration on the most discriminative regions. Finally, we set cluster size of 2,000 mm^3 to better visualize the most discriminative features of each metric.

RESULTS

Classification results

The prediction results of the fused classifier and the three base classifiers (GMV-based, FA-based and MD-based), as evaluated by LOOCV and 10-fold cross-validation, are summarized in Table 2. According to the LOOCV, the fused classifier yielded a classification accuracy of 83.59% with a significance of $p < 0.001$ revealed by a permutation test. The sensitivity and specificity were 78.13% and 89.06%, whereas the PPV and NPV were 87.72% and 80.28%. These results were better than the values obtained from the classifiers based on any single metric, which suggests that integrating sMRI and DTI was advantageous in identifying aMCI patients. The 10-fold cross-validation yielded the average classification accuracies of the fused classifier, GMV-based classifier, FA-based classifier and MD-based classifier of 83.70%, 77.91%, 74.26% and 79.59%, respectively. These results were similar to those of the LOOCV, which indicates the robustness of our results.

Table 2
Prediction results of the fused classifier and the three base classifiers evaluated by LOOCV and 10-fold cross-validation

	Accuracy (%)	Sensitivity (%)	Specificity (%)	PPV (%)	NPV (%)
LOOCV					
Fused	83.59%	78.13%	89.06%	87.72%	80.28%
GMV-based	76.56%	75.00%	78.13%	77.42%	75.76%
FA-based	75.78%	68.75%	82.81%	80.00%	72.60%
MD-based	78.91%	71.88%	85.94%	83.64%	75.34%
10-fold					
Fused	83.70%	78.64%	88.75%	87.55%	80.61%
GMV-based	77.65%	75.11%	80.19%	79.18%	76.34%
FA-based	74.65%	69.64%	79.66%	77.41%	72.42%
MD-based	79.46%	73.13%	85.80%	83.80%	76.16%

The ROC curves for the fused classifier and the single-metric based classifiers are shown in Fig. 2A. The AUC of the fused classifier was 0.862, which a permutation test demonstrate was significantly higher than chance ($p < 0.001$). The GMV-based, FA-based and MD-based classifiers were 0.823, 0.786 and 0.856, respectively.

Figure 2B displays the classification scores for all subjects. The positive scores denote aMCI individuals, and the negative scores denote the controls. As shown in the figure, 14 aMCI patients were misclassified as controls, and 7 controls were misclassified as aMCI patients. The classification scores were significantly correlated with performance on the MMSE ($r = -0.382, p < 0.0001$) across all subjects, which supports the validity of the fused classifier. Within each group, there were no such significant correlations (aMCI, $p = 0.833$; control, $p = 0.503$).

Discrimination maps of aMCI-specific abnormalities

GMVs acquired from the sMRI and the FAs/MDs acquired from the DTI were used to train the three base classifiers. The discrimination maps, i.e., the spatially distributed patterns of regions with the greatest contributions to the discrimination weights, for each base classifier are illustrated in Fig. 3, detailed in Table 3 and described below. Each discrimination map is a spatial representation of the SVM weight vector and shows the relative contribution of each voxel to the classification. The maps suggest there are abnormalities of GM or WM in aMCI patients compared to the NCs.

GMV-based classifier

The discriminative GMV pattern for classifying the aMCI and the NC groups included the following regions in both hemispheres: the inferior temporal gyrus, the superior temporal gyrus, the Heschl gyrus, the inferior frontal gyrus, the middle frontal gyrus, the thalamus, the angular gyrus, the inferior parietal lobule, the hippocampus, and the parahippocampal

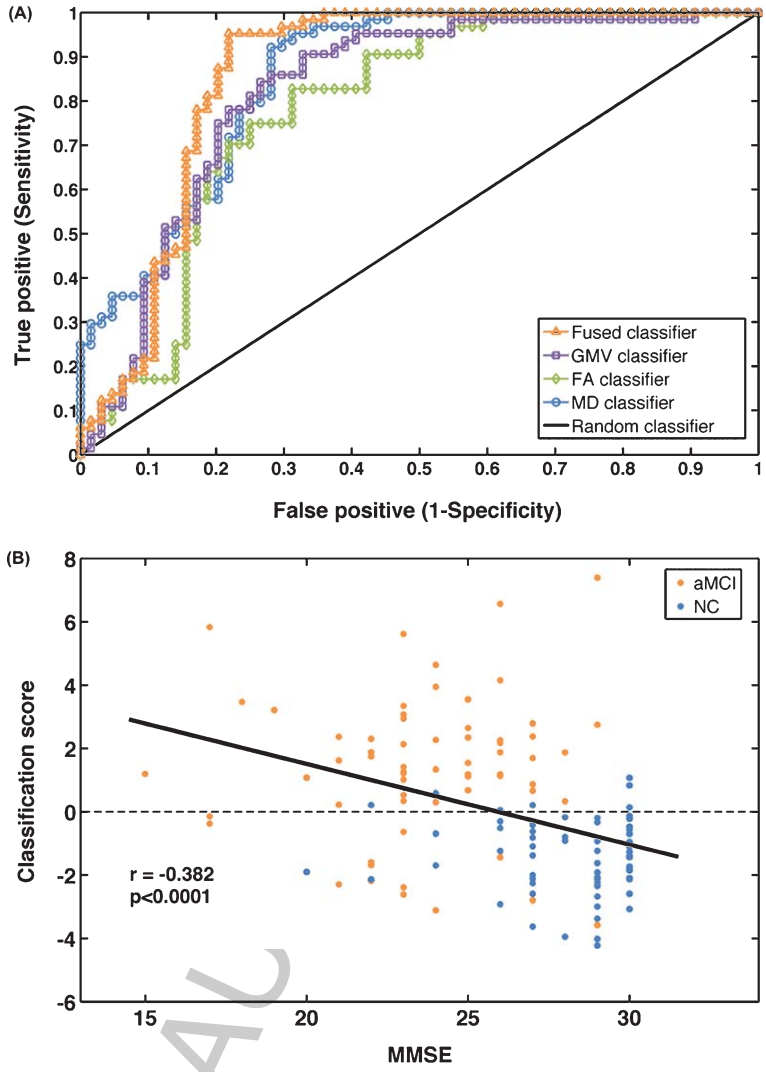

Fig. 2. Classification performance. A) The ROC curves for the fused, GMV-based, FA-based, and MD-based classifiers. AUC of the fused, GMV-based, FA-based, and MD-based classifiers were 0.862, 0.823, 0.786, and 0.856, respectively. B) Scatter plot of the classification scores of all subjects for the fused classifier. Here, individuals with positive scores were classified as aMCI, and individuals with negative scores were classified as NC. There is a significant correlation between the classification scores (distance from the hyperplane) and the MMSE scores across all subjects.

gyrus; the following left hemisphere regions: the middle temporal gyrus, the supramarginal gyrus, the amygdala, the cerebellum, the inferior occipital gyrus, the insula, and the middle occipital gyrus; and the following right hemisphere regions: the precuneus, the posterior cingulate gyrus, the gyrus rectus, the superior frontal gyrus, the temporal pole, and the Rolandic operculum.

FA-based classifier

The FA discriminative pattern included the following bilateral regions: the body of corpus callosum, the superior parietal blade, the parieto-temporal blade, the anterior corona radiata, the superior frontal blade, the posterior thalamic radiation, and the occipital blade; the following left hemisphere regions: the posterior corona radiata, the superior corona radiata; and the following right hemisphere regions: the cingulum (cingulate gyrus), the middle frontal blade, the inferior frontal blade, the retrolenticular part of internal capsule, and the inferior fronto-occipital fasciculus.

MD-based classifier

The MD discriminative pattern consisted of the following bilateral regions: the body of corpus callosum,

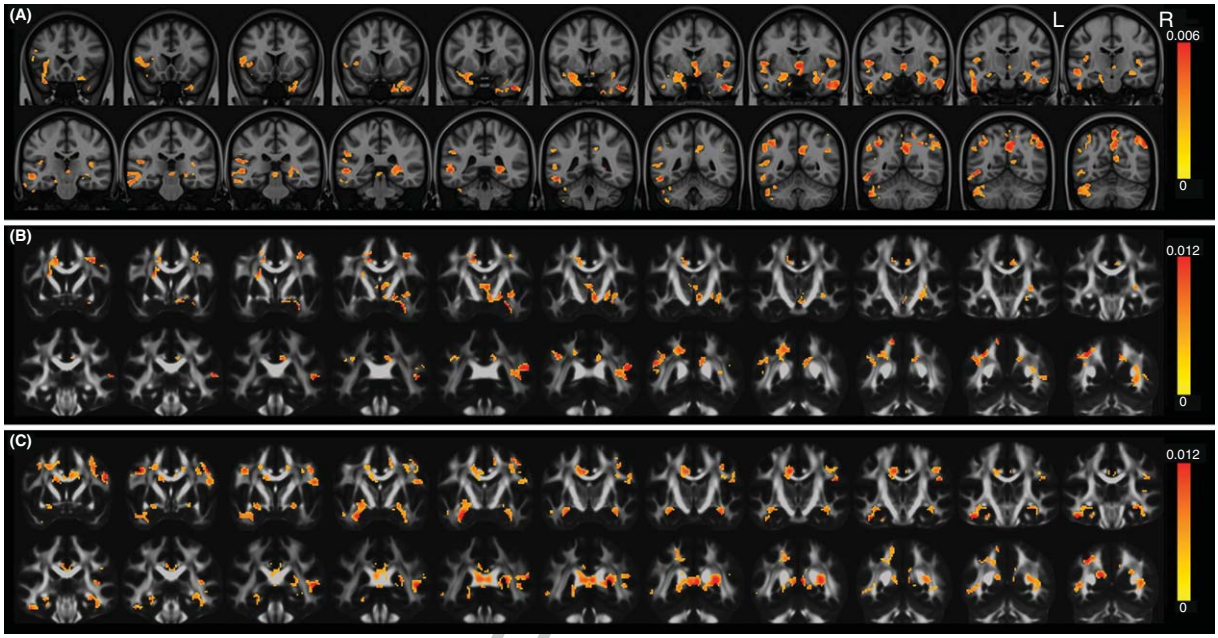

Fig. 3. Regions exhibiting high discrimination weights between the aMCI and control groups. A) GMV discrimination map. B) FA discrimination map. C) MD discrimination map.

the genu of corpus callosum, the splenium of corpus callosum, the temporal blade, the occipital blade, the superior frontal blade, and the middle frontal blade; the following left hemisphere regions: the cingulum (cingulate gyrus), the cingulum (hippocampus), the superior corona radiata, and the superior parietal blade; and the following right hemisphere regions: the posterior thalamic radiation, the pre-central blade, the post-central blade, the inferior frontal blade, the crus of the fornix, and the parieto-temporal blade.

DISCUSSION

Based on the whole-brain GMV, FA, and MD maps derived from sMRI and DTI, the current study presents a multivariate classification framework for distinguishing aMCI patients from normal controls that achieved good discriminative power (accuracy: 83.59%; sensitivity: 78.13%; and specificity: 89.06%). Interestingly, widespread GM and WM regions made a substantial contribution to this discrimination.

To date, very few studies have combined sMRI and DTI to identify aMCI patients. To our knowledge, only Cui and colleagues have combined subcortical volumetric measures and the FAs of several WM regions to classify aMCI and NC groups [11]. In contrast, the analyses in our study were conducted using whole-brain voxel-based maps of GMV, FA and MD. This approach led to greatly improved prediction power. These findings imply the substantial contributions of the brain regions that were excluded by Cui et al. [11] to aMCI classification.

Identification of aMCI using neuroimaging markers

Currently, the diagnosis of aMCI primarily relies on behavioral assessment. One primary drawback of the present approach to diagnosis is that the behavioral phenotypes of aMCI can be contaminated by other psychological and psychiatric disorders. Additionally, cognitive reserve might hide the representative behavioral symptoms of aMCI to some extent [29]. Therefore, objective biomarkers that are less affected by cognitive reserve are necessary for aMCI diagnosis. In this study, a multi-modal MRI-based classifier was proposed that could correctly classify 83.59% of all cases with a sensitivity of 78.13% and a specificity of 89.06% as evaluated by LOOCV. Notably, the consistent classification performance was acquired when the 10-fold cross-validation was applied for evaluation, which indicates the robustness of our results (Table 2). The good and stable classification performance of this system indicates that this approach will have diagnostic value in clinical settings.

Table 3
Regions exhibiting high discrimination weights between the aMCI and control groups in terms of GMV, FA, and MD

Metric	Region	size	x	y	z	w
GMV						
	Middle temporal gyrus L Inferior temporal gyrus L Superior temporal gyrus L Heschl gyrus L	2973	+54.0	+37.5	−1.5	0.0062
	Precuneus R Posterior cingulate gyrus R	2102	−6.0	+66.0	+57.0	0.0071
	Inferior frontal gyrus, orbital part L Inferior frontal gyrus, triangular part L Inferior frontal gyrus, opercular part L Insula L	1887	+42.0	−28.5	+1.5	0.0074
	Angular gyrus L Inferior parietal L Middle occipital L Supramarginal gyrus L	1877	+40.5	+54.0	+40.5	0.0070
	Amygdala L Hippocampus L Parahippocampal gyrus L	1389	+12.0	+3.0	−31.5	0.0055
	Gyrus rectus R Superior frontal gyrus, orbital part R Middle frontal gyrus, orbital part L	1389	−6.0	−52.5	−19.5	0.0057
	Cerebellum Crus1 L Cerebellum 6 L	1314	+52.5	+54.0	−37.5	0.0062
	Angular gyrus R Inferior parietal R	1308	−37.5	+73.5	+46.5	0.0072
	Inferior temporal R	1251	−45.0	−4.5	−34.5	0.0092
	Hippocampus R Parahippocampal gyrus R	1221	−24.0	+42.0	+3.0	0.0061
	Inferior temporal gyrus L Middle temporal gyrus L Inferior occipital gyrus L	1189	+39.0	+79.5	−7.5	0.0078
	Thalamus	898	−3.0	+7.5	−1.5	0.0071
	Middle frontal gyrus R Inferior frontal gyrus, orbital part R	872	−39.0	−42.0	−3.0	0.0064
	Superior temporal gyrus R Heschl gyrus R Rolandic operculum R	759	−51.0	+4.5	+3.0	0.0051
	Temporal pole: middle temporal gyrus R Temporal pole: superior temporal gyrus R	713	−21.0	−10.5	−33.0	0.0055
FA						
	Posterior corona radiata L Superior parietal blade L Parieto-temporal blade L	565	+32.0	+58.0	+40.0	0.019
	Body of corpus callosum Anterior corona radiata L Superior corona radiata L Superior frontal blade L	537	+14.0	+4.0	+40.0	0.014
	Cingulum. (cingulate gyrus) R Superior parietal blade	415	−14.0	+72.0	+40.0	0.019
	Posterior thalamic radiation R Occipital blade R	282	−38.0	+72.0	+8.0	0.013
	Middle frontal blade R	281	−36.0	+2.0	+46.0	0.013
	Anterior corona radiata R Inferior frontal blade R	279	−28.0	−28.0	−4.0	0.011
	Retrolenticular part of internal capsule R Inferior fronto-occipital fasciculus R	277	−28.0	+4.0	−20.0	0.016
	Posterior thalamic radiation L Occipital blade L	271	+36.0	+66.0	+10.0	0.010
	Anterior corona radiata R Superior frontal blade R	267	−12.0	−42.0	+26.0	0.013
	Parieto-temporal blade R	261	−50.0	+42.0	+22.0	0.019

(Continued)

Table 3
(*Continued*)

Metric	Region	size	x	y	z	w
MD						
	Splenium of corpus callosum Temporal blade L Occipital blade L Cingulum (hippocampus) L	1834	+44.0	+22.0	−24.0	0.016
	Genu of corpus callosum Body of corpus callosum Superior corona radiata L Cingulum (cingulate gyrus) L	1374	+2.0	−12.0	+26.0	0.014
	Posterior thalamic radiation R Occipital blade R Splenium of corpus callosum Tapetum R	738	−38.0	+72.0	+8.0	0.018
	Pre-central blade R Post-central blade R	448	−44.0	+6.0	+46.0	0.014
	Superior frontal blade L Middle frontal blade L	431	+40.0	−2.0	+38.0	0.016
	Middle frontal blade R	377	−32.0	−18.0	+46.0	0.014
	Superior frontal blade R Inferior frontal blade R	372	−36.0	−46.0	−2.0	0.022
	Crus of fornix R Temporal blade R	357	−34.0	+12.0	−18.0	0.010
	Body of corpus callosum Superior frontal blade R	328	−10.0	−36.0	+42.0	0.012
	Superior parietal blade L	257	+32.0	+58.0	+40.0	0.014
	Parieto-temporal blade R	253	−48.0	+36.0	+8.0	0.016

L, left; R, right.

It has been established that different parameters extracted from various modalities complement each other, and these parameters will always provide more comprehensive characterization of brain abnormalities when they are combined [18, 30]. In our study, GMV, FA, and MD were combined as classification features. The combined features resulted in greater classification accuracy than either feature alone (Table 2), which suggests that the three metrics are complementary when used for classifying aMCI and NC groups. Many prior studies have similarly revealed that aMCI is accompanied by GM abnormalities and WM integrity alterations [8, 10]. More generally, the good classification results of the combined classifier validated the value of integrating multi-modal parameters for classification.

GM and WM abnormalities in aMCI

GM discriminative regions

The following GM regions made the greatest contributions and have consistently exhibited abnormalities in previous studies: precuneus and insula [8, 31], posterior cingulate gyrus [31, 32], hippocampus [9, 33], parahippocampal gyrus [34, 35], superior temporal gyrus [4, 36], inferior temporal gyrus [37, 38], middle temporal gyrus [38], temporal pole [39], superior frontal gyrus [38], inferior frontal gyrus [12, 38], middle frontal gyrus [40], supramarginal gyrus [39, 41], angular gyrus [39], inferior parietal lobule [38, 42], amygdala and thalamus [43], occipital gyrus [5, 42], and cerebellum [44].

Specifically, the temporal lobe, precuneus, and posterior cingulate gyrus abnormalities were the most obvious when the GMVs were used to identify the aMCI patients. Abnormal regions with high discriminative weights were present in the medial temporal lobe, precuneus, and posterior cingulate gyrus, and these areas participate in the encoding, storage, or retrieval of episodic memories [45–47]. Moreover, the frontal lobe is also involved in the encoding and retrieval of episodic memory and the dysfunctions of the frontal lobe in aMCI may play a role in episodic memory impairment [47, 48]. Additionally, we also observed abnormalities in the cerebellum, which plays a significant role in sensorimotor control in cognition and affect and might impact executive function [49, 50]. Significant GMV reductions in the gyrus rectus have been observed in the brains of AD patients [51] but not in the brains of patients with early stage AD (i.e., aMCI). aMCI patients are known to have a greater tendency to progress to AD, which might

suggest that some aMCI patients already exhibited certain anomalies in regions with alterations that can only be observed in AD patients (e.g., the gyrus rectus).

WM discriminative regions

The WM regions selected by our method included the regions with abnormal FAs or MDs, and similar findings have been reported in several previous studies. The most discriminative WM regions revealed by FA include the superior parietal blade, parieto-temporal blade, frontal blade, cingulum, occipital blade [52, 53], corona radiata, body of the corpus callosum, internal capsule, posterior thalamic radiation [54], and right inferior fronto-occipital fasciculus [53]. The MD discrimination map consists of the corpus callosum, frontal blade, temporal blade, occipital blade, parieto-temporal blade, left cingulum (cingulate gyrus and hippocampus) [52], crus of the fornix [11, 53], left superior corona radiata, posterior thalamic radiation [54], right pre-central blade, and post-central blade [55].

We observed obvious WM disruptions in the corpus callosum, cingulum (cingulate gyrus and hippocampus), corona radiata, frontal lobe, and parietal lobe in the aMCI patients. Specifically, the corpus callosum and cingulum are the most commonly damaged areas in the WM pathways in aMCI patients and are also important parts of the Papez circuit [56], which is involved in short-term memory. Additionally, the frontal and parietal lobes are associated with the working memory [57]. WM lesions in these regions are closely related to memory impairment symptoms. Moreover, the parietal WM has a strong structural connection with extensive regions and plays an important role in language and semantic processing, spatial attention, orientation, and verbally mediated fact retrieval [58].

Pathological mechanism of GM/WM discrimination in aMCI

Notably, the different measures reflect different neuropathological and neurophysiological processes, and the region- and parameter-dependent variations might reflect the pathology/pathophysiology of aMCI. GMV mainly reflects the number of neurons within an ontogenetic column, and our results might be indicative of cellular changes in the discriminative GM regions in aMCI. Our discrimination maps revealed that the GM discriminative regions in aMCI were mainly located in the medial temporal lobe, temporal lobe, cingulate gyrus, parietal lobe, and frontal lobe. These findings correlate with the pathological process of AD. The early loss of neurons begins in the medial temporal lobe and gradually extends to the parietal and frontal cortices and suggests the degeneration and degradation of synapse-associated cortical pathways [59].

In contrast, FA reflects the degree of diffusion anisotropy that is determined by the fiber diameter and density and the degree of myelination, whereas MD can indirectly reflect the extracellular space, which is related to the density of the nerve fibers [60]. Decreased FA and increased MD always indicate impaired WM fiber tract integrity [61]. We found that the areas that made the greatest contributions to the classification in terms of both FA and MD included the body of corpus callosum, left superior parietal blade, superior corona radiata, right parieto-temporal blade, middle frontal blade, inferior frontal blade, posterior thalamic radiation, bilateral superior frontal blade, and occipital blade. These findings indicate that myelin or oligodendrocyte damage was present in these areas and led to degenerative changes in the myelinated nerve fiber bundles that further affected the cognitive activities of the patients [62]. Additionally, we observed that the most discriminative MD regions were more extensive than the most discriminative FA regions (Fig. 3). Therefore, MD might be more sensitive than FA in the detection of the early changes of WM microstructures in prodromal AD [63]. Therefore, it can be speculated that there might be greater changes in the absolute dimensions of the diffusion ellipsoid than in the shape of the diffusion ellipsoid in the very early stage of AD, and this speculation agrees with the findings of previous studies [63, 64].

Several studies have reported that abnormal WM tracts are related to GM abnormalities in AD [65, 66]. In this study, we also found several GM discriminative regions that were distributed symmetrically in both sides. These findings might be related to the corpus callosum, which contains the largest group of association fibers that pass between the left and right hemispheres. However, the relationship between WM and GM changes in aMCI is controversial, and our results did not reveal very strong positional congruent correlations between the WM and GM discriminative regions (Fig. 3). Therefore, we speculated that partial relationships between WM and GM abnormalities could not reflect the causality as has been suggested in some previous studies [10, 65, 67]. WM regions with alterations and GMV abnormal regions in aMCI patients were not entirely consistent. For example, the WM alterations more severe than GM abnormalities in the frontal lobe, whereas the opposite trend occurred in the rear section of the brain (Fig. 3). These findings support the idea that the WM damage pattern is different

from the GM pattern in early AD, and oligodendrocytes in regions where the myelin is formed later are more easily damaged by free radicals and other metabolites. Therefore, the WM in these regions is also the first WM to become involved in early AD [68].

Limitations

Although the proposed classification framework achieved good aMCI identification accuracy, several limitations of the present study should be noted. First, whereas the leave-one-out and 10-fold cross-validations were both used to evaluate the performance of our method and somewhat validated the robustness and stability of our results, these results need to be validated with an independent data set in the future. Second, only sMRI and DTI were combined in the present study and additional more neuroimaging modalities, such as resting state functional MRI, can be further integrated and might further improve the classification accuracy. Third, the present study was based on cross-sectional datasets. Longitudinal follow-up studies should be conducted to further validate our results. Finally, given substantial false positive and false negative results in our study, the interpretation of the most discriminative regions should be taken into account with caution.

CONCLUSIONS

Based on the structural MRI and DTI data, the current study proposed a method for identifying aMCI patients that exhibited good accuracy (accuracy: 83.59%; sensitivity: 78.13%; and specificity: 89.06%). Our findings suggest that aMCI is characterized by a distributed pattern of GM abnormalities and WM alterations that have discriminative power and can reflect relevant pathological changes in the brain. These findings highlight the advantage of multi-modal feature integration for identifying aMCI.

ACKNOWLEDGMENTS

This work was supported by CHINA-CANADA Joint Initiative on Alzheimer's Disease and Related Disorders (812111340), the National Science and Technology Major Projects for "Major New Drug Innovation and Development" of the Twelfth 5-year Plan Period (2011ZX09307-001-02), as well as the National Natural Science Foundation of China (Grant Nos. 30970823, 31371007, 81322021), the Beijing Nova Program (no. Z121110002512032) and Beijing Municipal Science & Technology Commission (Grant No. Z131100006813022), the Specialized Research Fund for the Doctoral Program of Higher Education, China (no. 20130003110002) and National Key Department of Neurology funded by Chinese Health and Family Planning Committee.

Authors' disclosures available online (http://j-alz.com/manuscript-disclosures/15-0184r1).

REFERENCES

[1] Lobo A, Launer LJ, Fratiglioni L, Andersen K, Di Carlo A, Breteler MM, Copeland JR, Dartigues JF, Jagger C, Martinez-Lage J, Soininen H, Hofman A (2000) Prevalence of dementia and major subtypes in Europe: A collaborative study of population-based cohorts. Neurologic Diseases in the Elderly Research Group. *Neurology* **54**, S4-9.

[2] Jia J, Wang F, Wei C, Zhou A, Jia X, Li F, Tang M, Chu L, Zhou Y, Zhou C, Cui Y, Wang Q, Wang W, Yin P, Hu N, Zuo X, Song H, Qin W, Wu L, Li D, Jia L, Song J, Han Y, Xing Y, Yang P, Li Y, Qiao Y, Tang Y, Lv J, Dong X (2014) The prevalence of dementia in urban and rural areas of China. *Alzheimers Dement* **10**, 1-9.

[3] Petersen RC, Thomas RG, Grundman M, Bennett D, Doody R, Ferris S, Galasko D, Jin S, Kaye J, Levey A, Pfeiffer E, Sano M, van Dyck CH, Thal LJ, Alzheimer's Disease Cooperative Study G (2005) Vitamin E and donepezil for the treatment of mild cognitive impairment. *N Engl J Med* **352**, 2379-2388.

[4] Li S, Yuan X, Pu F, Li D, Fan Y, Wu L, Chao W, Chen N, He Y, Han Y (2014) Abnormal changes of multidimensional surface features using multivariate pattern classification in amnestic mild cognitive impairment patients. *J Neurosci* **34**, 10541-10553.

[5] Wee CY, Yap PT, Shen D (2012) Prediction of Alzheimer's disease and mild cognitive impairment using cortical morphological patterns. *Hum Brain Mapp* **34**, 3411-3425.

[6] Haller S, Nguyen D, Rodriguez C, Emch J, Gold G, Bartsch A, Lovblad KO, Giannakopoulos P (2010) Individual prediction of cognitive decline in mild cognitive impairment using support vector machine-based analysis of diffusion tensor imaging data. *J Alzheimers Dis* **22**, 315-327.

[7] Wee CY, Yap PT, Li W, Denny K, Browndyke JN, Potter GG, Welsh-Bohmer KA, Wang L, Shen D (2011) Enriched white matter connectivity networks for accurate identification of MCI patients. *Neuroimage* **54**, 1812-1822.

[8] Misra C, Fan Y, Davatzikos C (2009) Baseline and longitudinal patterns of brain atrophy in MCI patients, and their use in prediction of short-term conversion to AD: Results from ADNI. *Neuroimage* **44**, 1415-1422.

[9] Pennanen C, Kivipelto M, Tuomainen S, Hartikainen P, Hanninen T, Laakso MP, Hallikainen M, Vanhanen M, Nissinen A, Helkala EL, Vainio P, Vanninen R, Partanen K, Soininen H (2004) Hippocampus and entorhinal cortex in mild cognitive impairment and early AD. *Neurobiol Aging* **25**, 303-310.

[10] Selnes P, Fjell AM, Gjerstad L, Bjornerud A, Wallin A, Due-Tonnessen P, Grambaite R, Stenset V, Fladby T (2012) White matter imaging changes in subjective and mild cognitive impairment. *Alzheimers Dement* **8**, S112-S121.

[11] Cui Y, Wen W, Lipnicki DM, Beg MF, Jin JS, Luo S, Zhu W, Kochan NA, Reppermund S, Zhuang L, Raamana PR, Liu T, Trollor JN, Wang L, Brodaty H, Sachdev PS (2012) Automated detection of amnestic mild cognitive impairment in

community-dwelling elderly adults: A combined spatial atrophy and white matter alteration approach. *Neuroimage* **59**, 1209-1217.

[12] Han Y, Wang J, Zhao Z, Min B, Lu J, Li K, He Y, Jia J (2011) Frequency-dependent changes in the amplitude of low-frequency fluctuations in amnestic mild cognitive impairment: A resting-state fMRI study. *Neuroimage* **55**, 287-295.

[13] Ashburner J, Friston KJ (2005) Unified segmentation. *Neuroimage* **26**, 839-851.

[14] Ashburner J (2007) A fast diffeomorphic image registration algorithm. *Neuroimage* **38**, 95-113.

[15] Cui Z, Zhong S, Xu P, He Y, Gong G (2013) PANDA: A pipeline toolbox for analyzing brain diffusion images. *Front Hum Neurosci* **7**, 42.

[16] De Martino F, Valente G, Staeren N, Ashburner J, Goebel R, Formisano E (2008) Combining multivariate voxel selection and support vector machines for mapping and classification of fMRI spatial patterns. *Neuroimage* **43**, 44-58.

[17] Pereira F, Mitchell T, Botvinick M (2009) Machine learning classifiers and fMRI: A tutorial overview. *Neuroimage* **45**, S199-S209.

[18] Dai ZJ, Yan CG, Wang ZQ, Wang JH, Xia MR, Li KC, He Y (2012) Discriminative analysis of early Alzheimer's disease using multi-modal imaging and multi-level characterization with multi-classifier (M3). *Neuroimage* **59**, 2187-2195.

[19] Dosenbach NUF, Nardos B, Cohen AL, Fair DA, Power JD, Church JA, Nelson SM, Wig GS, Vogel AC, Lessov-Schlaggar CN (2010) Prediction of individual brain maturity using fMRI. *Science* **329**, 1358-1361.

[20] Vapnik V (2000) *The Nature of Statistical Learning Theory,* Springer.

[21] Chang CC, Lin CJ (2011) LIBSVM: A Library for Support Vector Machines. *Acm T Intel Syst Tec* **2**, 27.

[22] Kittler J, Hatef M, Duin RPW, Matas J (1998) On combining classifiers. *IEEE T Pattern Anal* **20**, 226-239.

[23] Polikar R (2006) Ensemble based systems in decision making. *IEEE Circ Syst Mag* **6**, 21-45.

[24] Kuncheva LI (2007) Combining pattern classifiers: Methods and algorithms (kuncheva, li; 2004)[book review]. *IEEE T Neural Networ* **18**, 964-964.

[25] Ross A, Jain A (2003) Information fusion in biometrics. *Pattern Recogn Lett* **24**, 2115-2125.

[26] Fawcett T (2006) An introduction to ROC analysis. *Pattern Recogn Lett* **27**, 861-874.

[27] Ecker C, Marquand A, Mourao-Miranda J, Johnston P, Daly EM, Brammer MJ, Maltezos S, Murphy CM, Robertson D, Williams SC, Murphy DG (2010) Describing the brain in autism in five dimensions–magnetic resonance imaging-assisted diagnosis of autism spectrum disorder using a multiparameter classification approach. *J Neurosci* **30**, 10612-10623.

[28] Mourao-Miranda J, Bokde AL, Born C, Hampel H, Stetter M (2005) Classifying brain states and determining the discriminating activation patterns: Support Vector Machine on functional MRI data. *Neuroimage* **28**, 980-995.

[29] Querbes O, Aubry F, Pariente J, Lotterie JA, Démonet JF, Duret V, Puel M, Berry I, Fort JC, Celsis P (2009) Early diagnosis of Alzheimer's disease using cortical thickness: Impact of cognitive reserve. *Brain* **132**, 2036-2047.

[30] Liu F, Wee CY, Chen H, Shen D (2014) Inter-modality relationship constrained multi-modality multi-task feature selection for Alzheimer's disease and mild cognitive impairment identification. *Neuroimage* **84**, 466-475.

[31] Davatzikos C, Bhatt P, Shaw LM, Batmanghelich KN, Trojanowski JQ (2011) Prediction of MCI to AD conversion. via MRI, CSF biomarkers, and pattern classification. *Neurobiol Aging* **32**, 2322.e19-e27.

[32] Han Y, Lui S, Kuang W, Lang Q, Zou L, Jia J (2012) Anatomical and functional deficits in patients with amnestic mild cognitive impairment. *PLoS One* **7**, e28664.

[33] Bell-McGinty S, Lopez OL, Meltzer CC, Scanlon JM, Whyte EM, Dekosky ST, Becker JT (2005) Differential cortical atrophy in subgroups of mild cognitive impairment. *Arch Neurol* **62**, 1393-1397.

[34] Celone KA, Calhoun VD, Dickerson BC, Atri A, Chua EF, Miller SL, DePeau K, Rentz DM, Selkoe DJ, Blacker D, Albert MS, Sperling RA (2006) Alterations in memory networks in mild cognitive impairment and Alzheimer's disease: An independent component analysis. *J Neurosci* **26**, 10222-10231.

[35] Machulda MM, Senjem ML, Weigand SD, Smith GE, Ivnik RJ, Boeve BF, Knopman DS, Petersen RC, Jack CR Jr (2009) Functional MRI changes in amnestic and non-amnestic MCI during encoding and recognition tasks. *J Int Neuropsych Soc* **15**, 372.

[36] Wee CY, Yap PT, Zhang D, Denny K, Browndyke JN, Potter GG, Welsh-Bohmer KA, Wang L, Shen D (2012) Identification of MCI individuals using structural and functional connectivity networks. *Neuroimage* **59**, 2045-2056.

[37] Lenzi D, Serra L, Perri R, Pantano P, Lenzi GL, Paulesu E, Caltagirone C, Bozzali M, Macaluso E (2011) Single domain amnestic MCI: A multiple cognitive domains fMRI investigation. *Neurobiol Aging* **32**, 1542-1557.

[38] Liu Y, Paajanen T, Zhang Y, Westman E, Wahlund LO, Simmons A, Tunnard C, Sobow T, Mecocci P, Tsolaki M, Vellas B, Muehlboeck S, Evans A, Spenger C, Lovestone S, Soininen H, AddNeuroMed C (2011) Combination analysis of neuropsychological tests and structural MRI measures in differentiating AD, MCI and control groups–the AddNeuroMed study. *Neurobiol Aging* **32**, 1198-1206.

[39] Karas G, Sluimer J, Goekoop R, van der Flier W, Rombouts SA, Vrenken H, Scheltens P, Fox N, Barkhof F (2008) Amnestic mild cognitive impairment: Structural MR imaging findings predictive of conversion to Alzheimer disease. *AJNR Am J Neuroradiol* **29**, 944-949.

[40] Wang L, Goldstein FC, Veledar E, Levey AI, Lah JJ, Meltzer CC, Holder CA, Mao H (2009) Alterations in cortical thickness and white matter integrity in mild cognitive impairment measured by whole-brain cortical thickness mapping and diffusion tensor imaging. *AJNR Am J Neuroradiol* **30**, 893-899.

[41] Desikan RS, Cabral HJ, Hess CP, Dillon WP, Glastonbury CM, Weiner MW, Schmansky NJ, Greve DN, Salat DH, Buckner RL, Fischl B, Alzheimer's Disease Neuroimaging I (2009) Automated MRI measures identify individuals with mild cognitive impairment and Alzheimer's disease. *Brain* **132**, 2048-2057.

[42] Liu M, Zhang D, Shen D, Alzheimer's Disease Neuroimaging I (2012) Ensemble sparse classification of Alzheimer's disease. *Neuroimage* **60**, 1106-1116.

[43] Zhang Y, Schuff N, Camacho M, Chao LL, Fletcher TP, Yaffe K, Woolley SC, Madison C, Rosen HJ, Miller BL, Weiner MW (2013) MRI markers for mild cognitive impairment: Comparisons between white matter integrity and gray matter volume measurements. *PLoS One* **8**, e66367.

[44] Spulber G, Niskanen E, Macdonald S, Kivipelto M, Padilla DF, Julkunen V, Hallikainen M, Vanninen R, Wahlund LO, Soininen H (2012) Evolution of global and local grey matter atrophy on serial MRI scans during the progression from MCI to AD. *Curr Alzheimer Res* **9**, 516-524.

[45] Minoshima S, Giordani B, Berent S, Frey KA, Foster NL, Kuhl DE (1997) Metabolic reduction in the posterior cingulate cortex in very early Alzheimer's disease. *Ann Neurol* **42**, 85-94.
[46] Cavanna AE, Trimble MR (2006) The precuneus: A review of its functional anatomy and behavioural correlates. *Brain* **129**, 564-583.
[47] Simons JS, Spiers HJ (2003) Prefrontal and medial temporal lobe interactions in long-term memory. *Nat Rev Neurosci* **4**, 637-648.
[48] Fletcher P, Henson RNA (2001) Frontal lobes and human memory insights from functional neuroimaging. *Brain* **124**, 849-881.
[49] Colloby SJ, O'Brien JT, Taylor JP (2014) Patterns of cerebellar volume loss in dementia with Lewy bodies and Alzheimers disease: A VBM-DARTEL study. *Psychiatry Res* **223**, 187-191.
[50] Schmahmann JD, Caplan D (2006) Cognition, emotion and the cerebellum. *Brain* **129**, 290-292.
[51] Frings L, Yew B, Flanagan E, Lam BY, Hull M, Huppertz HJ, Hodges JR, Hornberger M (2014) Longitudinal grey and white matter changes in frontotemporal dementia and Alzheimer's disease. *PLoS One* **9**, e90814.
[52] Sexton CE, Kalu UG, Filippini N, Mackay CE, Ebmeier KP (2011) A meta-analysis of diffusion tensor imaging in mild cognitive impairment and Alzheimer's disease. *Neurobiol Aging* **32**, 2322 e2325-2318.
[53] Bosch B, Arenaza-Urquijo EM, Rami L, Sala-Llonch R, Junque C, Sole-Padulles C, Pena-Gomez C, Bargallo N, Molinuevo JL, Bartres-Faz D (2012) Multiple DTI index analysis in normal aging, amnestic MCI and AD. Relationship with neuropsychological performance. *Neurobiol Aging* **33**, 61-74.
[54] Liu J, Yin C, Xia S, Jia L, Guo Y, Zhao Z, Li X, Han Y, Jia J (2013) White matter changes in patients with amnestic mild cognitive impairment detected by diffusion tensor imaging. *PLoS One* **8**, e59440.
[55] Li H, Liang Y, Chen K, Li X, Shu N, Zhang Z, Wang Y (2013) Different patterns of white matter disruption among amnestic mild cognitive impairment subtypes: Relationship with neuropsychological performance. *J Alzheimers Dis* **36**, 365-376.
[56] Papez JW (1937) A proposed mechanism of emotion. *Arch Neurol Psych* **38**, 725-743.
[57] Olesen PJ, Westerberg H, Klingberg T (2004) Increased prefrontal and parietal activity after training of working memory. *Nat Neurosci* **7**, 75-79.
[58] Uddin LQ, Supekar K, Amin H, Rykhlevskaia E, Nguyen DA, Greicius MD, Menon V (2010) Dissociable connectivity within human angular gyrus and intraparietal sulcus: Evidence from functional and structural connectivity. *Cereb Cortex* **20**, 2636-2646.
[59] Whitwell JL, Shiung MM, Przybelski SA, Weigand SD, Knopman DS, Boeve BF, Petersen RC, Jack CR Jr (2008) MRI patterns of atrophy associated with progression to AD in amnestic mild cognitive impairment. *Neurology* **70**, 512-520.
[60] Beaulieu C (2002) The basis of anisotropic water diffusion in the nervous system–a technical review. *NMR Biomed* **15**, 435-455.
[61] Assaf Y, Pasternak O (2008) Diffusion tensor imaging (DTI)-based white matter mapping in brain research: A review. *J Mol Neurosci* **34**, 51-61.
[62] Sjobeck M, Haglund M, Englund E (2005) Decreasing myelin density reflected increasing white matter pathology in Alzheimer's disease–a neuropathological study. *Int J Geriatr Psychiatry* **20**, 919-926.
[63] Wang Y, West JD, Flashman LA, Wishart HA, Santulli RB, Rabin LA, Pare N, Arfanakis K, Saykin AJ (2012) Selective changes in white matter integrity in MCI and older adults with cognitive complaints. *Biochim Biophys Acta* **1822**, 423-430.
[64] Acosta-Cabronero J, Williams GB, Pengas G, Nestor PJ (2010) Absolute diffusivities define the landscape of white matter degeneration in Alzheimer's disease. *Brain* **133**, 529-539.
[65] Agosta F, Pievani M, Sala S, Geroldi C, Galluzzi S, Frisoni GB, Filippi M (2011) White matter damage in Alzheimer disease and its relationship to gray matter atrophy. *Radiology* **258**, 853-863.
[66] Villain N, Desgranges B, Viader F, de la Sayette V, Mezenge F, Landeau B, Baron JC, Eustache F, Chetelat G (2008) Relationships between hippocampal atrophy, white matter disruption, and gray matter hypometabolism in Alzheimer's disease. *J Neurosci* **28**, 6174-6181.
[67] Salat DH, Tuch DS, van der Kouwe AJ, Greve DN, Pappu V, Lee SY, Hevelone ND, Zaleta AK, Growdon JH, Corkin S, Fischl B, Rosas HD (2010) White matter pathology isolates the hippocampal formation in Alzheimer's disease. *Neurobiol Aging* **31**, 244-256.
[68] Stricker NH, Schweinsburg BC, Delano-Wood L, Wierenga CE, Bangen KJ, Haaland KY, Frank LR, Salmon DP, Bondi MW (2009) Decreased white matter integrity in late-myelinating fiber pathways in Alzheimer's disease supports retrogenesis. *Neuroimage* **45**, 10-16.